Inorganic Chemistry

ARTICLE

pubs.acs.org/IC

# Growth of Piezoelectric Water-Free $GeO_2$ and $SiO_2$-Substituted $GeO_2$ Single-Crystals

A. Lignie, P. Armand,* and P. Papet

Institut Charles Gerhardt Montpellier, UMR5253, CNRS-UM2-ENSCM-UM1, C2M, UMII, CC1504, Place E. Bataillon, 34095 Montpellier Cedex 5, France

**ABSTRACT:** Using the slow-cooling method in selected fluxes, we have grown spontaneously nucleated single-crystals of pure $GeO_2$ and $SiO_2$-substituted $GeO_2$ materials with the α-quartz structure. These piezoelectric materials were obtained in millimeter size as well-faceted, visually colorless, and transparent crystals. Cubic-like or hexagonal prism-like morphology was identified depending on the chemical composition of the single-crystals and on the nature of the flux. Both the silicon substitution rate and the homogeneity of its distribution were estimated by Energy Dispersive X-ray spectroscopy. The cell parameters of the flux-grown $GeO_2$ and $Ge_{1-x}Si_xO_2$ ($0.038 \leq x \leq 0.089$) solid-solution were deduced from their X-ray powder diffraction pattern. As expected, the cell volumes decrease as the silicon content substitution increases. A room temperature Infrared spectroscopy study confirms the absence of hydroxyl groups in the as-grown crystals. Unlike what was observed for hydrothermally grown $GeO_2$ crystals, these flux-grown oxide materials did not present any phase transition before melting as pointed out by a Differential Scanning Calorimetry study. Neither a α-quartz/β-quartz transition as encountered in $SiO_2$ near 573 °C nor a α-quartz to rutile transformation were detected for these $GeO_2$ and $Ge_{1-x}Si_xO_2$ single-crystals.

## INTRODUCTION

In the $XO_2$ (X = Si, Ge) family, the quartz structure is composed by $XO_4$ corner-shared tetrahedra forming a trigonal system. The alpha-phase ($P3_121$ or $P3_221$, respectively left-handed or right-handed) is derived from the beta-phase ($P6_222$ or $P6_422$) by a symmetry loss induced by a tilt of the tetrahedra around the *b*-axis. Two distortion parameters exist to quantify this phenomenon: the intertetrahedral angle $\theta$ (X-O-X) and the tilt angle $\delta$.[1] The very promising piezoelectric properties of $GeO_2$ compared to $SiO_2$ would be directly related to its high angle distortion. Indeed, a linear relationship was found between the distortion parameters and the electromechanical coupling coefficient.[2]

In addition, the well-known α−β phase transition, which appears around 573 °C in $SiO_2$ ($\theta$ = 144.2°), does not occur when the tilt angle is over 22° (equivalent to $\theta$ under 136°).[3] In other words, the transition from an alpha piezoelectric phase to a beta nonpiezoelectric phase is absent for $GeO_2$ crystallized material ($\theta$ = 130.04°).[3]

The alpha-quartz form of $GeO_2$ is metastable in normal conditions of pressure and temperature.[4] Nonetheless, the kinetic of the allotropic transformation to the stable structure (rutile phase, $P4_2/mnm$) is extremely low, nonappreciable without the presence of any catalyst like chlorides or water.[5] Previous studies on thermal stability of α-$GeO_2$ powder showed conservation of the metastable structure until its fusion.[6]

Efforts to grow large single-crystals of α-$GeO_2$ were made, mainly by hydrothermal methods.[7−9] However, because of the use of aqueous media, hydroxyl groups were included in the $GeO_2$ crystals, catalyzing their return in the thermodynamically stable structure when heated to 180−200 °C. A thermal analysis of $SiO_2$-substituted $GeO_2$ crystals grown by a reflux method has shown that the quartz to rutile phase transformation is delayed with the increase of the silicon substitution.[9] The presence of Si atoms in the $GeO_2$ α-quartz-like structure will be an important factor to thermally stabilize this piezoelectric metastable phase.

This paper describes the use of the flux method to obtain water-free single-crystals of the metastable form of $GeO_2$ and of $GeO_2$−$SiO_2$ mixed compositions. The silicon substitution rate was estimated by Energy Dispersive X-ray (EDX) spectroscopy, and their room temperature structure analyzed by powder X-ray Diffraction (XRD). The thermal behavior of these flux-grown materials was characterized by Differential Scanning Calorimetry (DSC). The absence of hydroxyl groups in the as-grown crystals was confirmed by room temperature Infrared measurements registered in the transmittance mode.

## EXPERIMENTAL PROCEDURE

**Synthesis.** Glasses of pure $GeO_2$ and mixed $GeO_2$−$SiO_2$ solutions were used as solutes for the crystal growth experiments. The $GeO_2$−$SiO_2$ glasses were prepared from $SiO_2$ and $GeO_2$ commercial powders (Alfa Aesar 99.5% and Metaleurop 99.999% respectively) mixed in a Si/Ge molar ratio of 0.031, 0.053, and 0.111, heated above their melting temperature, that is, from 1230 to 1300 °C, held 2 h for homogenization, and ice-quenched to room temperature. The vitreous $GeO_2$ source was prepared by ice-quenching germanium dioxide that had been fused at 1200 °C for a couple of hours.

**Received:** March 31, 2011
**Published:** August 29, 2011

**Table 1. Selected Flux Compositions, Their Synthesis Temperature, and Their Corresponding Melting and Solidification Temperatures As Determined by DSC**

| | synthesis temperature (°C) | melting temperature (°C) | solidification temperature (°C) |
|---|---|---|---|
| $Li_2Mo_3O_{10}$ | 535 | 560 ± 1 | 378 ± 1 |
| $K_2Mo_2O_7$ | 450 | 499 ± 1 | 397 ± 1 |
| $K_2Mo_3O_{10}$ | 500 | 574 ± 1 | 497 ± 1 |
| $K_2Mo_4O_{13}$ | 510 | 567 ± 1 | 473 ± 1 |
| $Rb_2Mo_2O_7$ | 450 | 494 ± 1 | 410 ± 1 |
| $Rb_2Mo_3O_{10}$ | 500 | 581 ± 1 | 478 ± 1 |
| $Rb_2Mo_4O_{13}$ | 520 | 565 ± 1 | 492 ± 1 |
| $Cs_2Mo_2O_7$ | 410 | 467 ± 1 | 383 ± 1 |
| $Cs_2Mo_3O_{10}$ | 470 | 551 ± 1 | 459 ± 1 |
| $Cs_2Mo_4O_{13}$ | 470 | 539 ± 1 | 480 ± 1 |
| $K_2W_2O_7$ | 580 | 640 ± 1 | 596 ± 1 |

Several inorganic materials were tested as growth solvents (fluxes). On the basis of previous works, both the molybdate and the tungstate systems were preferred since they present low melting temperature and low evaporation at high temperatures.[10] All the inorganic compositions selected as potential fluxes for $GeO_2$ and $SiO_2$-substituted $GeO_2$ single-crystals are gathered in Table 1. Several compositions were selected in the $T_2O$-$MoO_3$ alkali molybdate systems with T = Li, K, Rb, Cs while only one composition was preferred in the $K_2O$-$WO_3$ binary system, $K_2W_2O_7$. They were synthesized via a solid-state reaction (50 °C below their melting point) during two weeks between the alkali carbonate $T_2CO_3$ (T = Li, K, Rb, Cs) and the corresponding oxide, $MoO_3$ or $WO_3$.

The principle of flux growth is based on the spontaneous nucleation that occurs when a supersaturation is obtained upon cooling of a high temperature solution. For the crystal growth experiments, a glass solute was thoroughly mixed with a selected flux respecting a solute to flux ratio of 10/90 in weight. A charge of 34 g (glass solute + flux) was placed in a 25 $cm^3$ Pt covered crucible and heated up to 970 °C during 24 h for homogenization. Then, the melted charge was slowly cooled down to 600 °C at a rate of 1 °C per hour without mechanical rotation. Finally, the muffle furnace equipped with an automatic temperature controller was turned off.

Back to room temperature, the solidified charge containing the crystals was mechanically extracted from the crucible and placed in chloride acid to dissolve the flux with the help of an ultrasonic bath cleaner. Once the flux dissolution was completed, the remaining crystals were washed several times in water and then in ethanol.

**Characterizations.** Powder XRD were performed at room temperature on an X′Pert Pro II diffractometer (PANalytical) equipped with a bichromatic Cu Kα radiation and a CCD detector. The scanning step width of 0.02° and the scanning rate of 0.00027° $s^{-1}$ were applied to record the patterns in the $2\theta$ range of 10−110°.

EDX analyses were set up on a Quanta 200 FEG (FEI) Scanning Electron Microscopy (SEM) equipped with an SDD diode as detector (Oxford INCA). Calibration was made with known elemental standards. The minimum detection limit depends on a first approximation on the chemical element. In our cases, the threshold detection of the Si atoms (minor element) in the $GeO_2$ matrix (major elements) is around 0.3%. Spectra were registered under low vacuum (around $10^{-3}$ Pa) at 15 kV. Several point analyses (at least three different areas checked) were performed on the as-grown single-crystals to ensure its homogeneity.

Fourier Transform Infrared Reflection spectroscopy (FT-IR) was performed in air on a IFS 66v spectrometer (Bruker) supplied with a detector MCT. Sample positioning was made with the help of a Hyperion microscope using a magnification of ×15.

The grown crystals were powdered with an average grain size of 20 μm and used for the DSC study. The thermal experiments were carried out using a Labsys calorimeter (Setaram instrumentation) in an inert atmosphere. Spectra were recorded at a heating rate of 2 °C/hour from ambient temperature to 1200 °C. The sample weight used was around 80 mg.

## RESULTS AND DISCUSSION

**Crystal Growth Experiments.** Pure $GeO_2$ and $SiO_2$-substituted $GeO_2$ single-crystals were obtained in the millimeter-size by spontaneous nucleation in an inorganic flux using the slow-cooling method. The whole growth experiments presented in this paper were done with the same experimental conditions to study the influence of the flux chemical composition on both the quality and the size of the as-grown crystals presenting the α-quartz structure. Another important parameter which was taken into account was the eventual presence of a second type of crystal such as, for example, the rutile-like form (stable form at room temperature). It is well-known that $GeO_2$ binary oxide is a good glass former. However, with our experimental growth conditions, the formation of bulk glassy materials as a result of the crystal growth experiments was never observed.

Concerning the pure $GeO_2$ material, well-faceted and visually colorless and transparent single-crystals were obtained in fluxes as $K_2Mo_4O_{13}$, $Rb_2Mo_4O_{13}$, and $Rb_2Mo_2O_7$. Therefore, it should be noticed that only few germanium oxide crystals were formed during each growth experiment.

The presented as-grown crystals have no visible flux inclusions or cracks, as illustrated by the photographs in Figure 1. These millimeter-size crystals present either a pseudocubic shape, Figures 1a and 1b, or an unshaped morphology, Figures 1b and 1c, with very smooth surface roughness.

The pseudocubic form was already found for the low-temperature phase of quartz.[11] The crystal habit of α-quartz has been well-established for a long time.[12] The three predominant crystal faces encountered in α-quartz crystals are the prism m $\{10\bar{1}0\}$, the negative z $\{01\bar{1}1\}$, and the positive r $\{10\bar{1}1\}$ rhombohedral faces.[12] These crystal-faces are of F-type from Hartman and Perdock's nomenclature of their Periodic Bond Chains method (PBC).[13] The habit of crystals grown freely in solution is usually determined by the slowly growing F-faces.[14] In the case of these pseudocubic crystals, m-faces are not present. We note the prevalent development of the rhombohedron r with the restricted presence of rhombohedron z, Figure 1a. The two types of faces differ in luster, the r faces being the most brilliant.

Pure $GeO_2$ crystals synthesized with $Cs_2Mo_4O_{13}$ flux were bigger in size, up to 4.2 × 2.5 × 1.2 $mm^3$, flux inclusions-free but they presented a rough surface and were not well shaped as shown in Figure 2a. The result of the experiments using $K_2W_2O_7$ flux was very poor, Figure 2b. The majority of the as-grown materials contain flux inclusions (which appear as yellow) resulting from unstable growth.[15]

As a result of the $GeO_2$ crystal growth experiments in $Rb_2Mo_3O_{10}$ and $Cs_2O$-$nMoO_3$, with $n$ = 2 and 3, two types of crystals were present (Figure 3): the colorless α-quartz $GeO_2$ and some amber tiny crystals, typically 0.5 × 0.3 × 0.2 $mm^3$ identified as the stable form of the material, that is, $GeO_2$ crystals with the rutile-like structure. It is believed that the color is due to oxygen deficiency.[16] However, the coloration was not removed after heating these amber rutile-like $GeO_2$ crystals for 1 week at 850 °C in air.


dx.doi.org/10.1021/ic200661q |Inorg. Chem. 2011, 50, 9311–9317

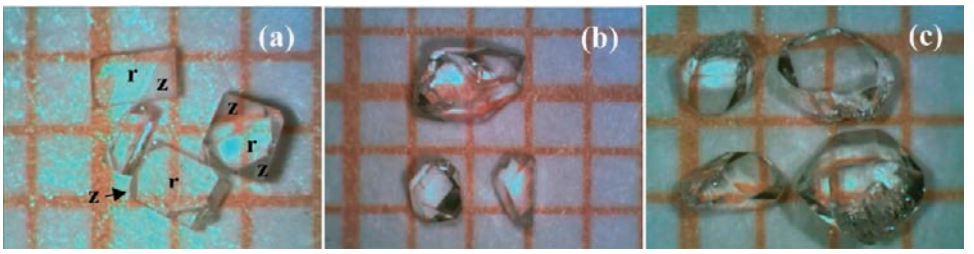


**Figure 1.** Photographs of as-grown $GeO_2$ single-crystals with uniform transparency grown in the different fluxes; (a) $Rb_2Mo_2O_7$, (b) $Rb_2Mo_4O_{13}$, and (c) $K_2Mo_4O_{13}$, (mm grid).

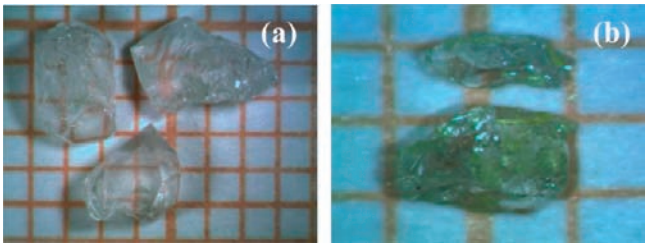


**Figure 2.** $GeO_2$ materials grown respectively in (a) $Cs_2Mo_4O_{13}$ and (b) $K_2W_2O_7$ flux, (mm grid).

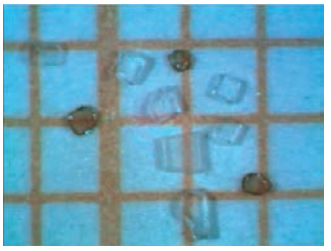

**Figure 3.** $GeO_2$ single-crystals: the amber rutile form and the colorless α-quartz phase, (mm grid).

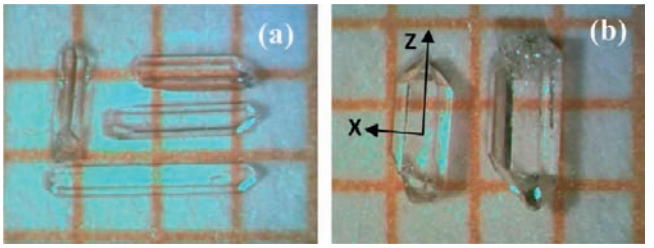


**Figure 4.** Photographs of as-grown low-$SiO_2$-substituted $GeO_2$ single-crystals in the different fluxes; (a) $Cs_2Mo_3O_{10}$ and (b) $Rb_2Mo_4O_{13}$, (mm grid).

The low-$SiO_2$-substituted $GeO_2$ single-crystals, obtained from a glass solute with a Si-content close to a $Ge_{0.97}Si_{0.03}O_2$ composition, show a well-developed morphology when obtained in $K_2Mo_4O_{13}$, $Rb_2Mo_4O_{13}$, and $Cs_2Mo_3O_{10}$ fluxes, Figure 4. Compared to the pure $GeO_2$ experiments, the yield of low-$SiO_2$-substituted $GeO_2$ crystals obtained was increased by a factor of 2 to 3.

Colorless, highly transparent, and flux-free single-crystals with a very smooth surface roughness were obtained, Figure 4. They present the most widespread of crystal forms; the hexagonal

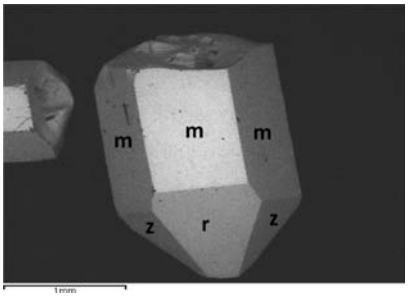


**Figure 5.** SEM photograph of a representative low-$SiO_2$-substituted $GeO_2$ single-crystal with the hexagonal prismatic morphology.

prism-like shape, typical of the α-phase of $SiO_2$, with cap faces on both ends for some of them.[17]

Some as-grown crystals are very slim, Figure 4a, with less than 0.4 mm in diameter and with length up to 2.5 mm in the *Z*-direction (optical axis) while others are about two times larger but shorter in length, Figure 4b. The directions are given with reference to the orthogonal axial system *XYZ* in which *X* and *Z* coincide with the *a* and *c* hexagonal axis respectively. The growth of these $SiO_2$-substituted $GeO_2$ crystals is rather anisotropic.

As already mentioned above, the three predominant crystal faces encountered in low-temperature quartz crystals are m $\{10\bar{1}0\}$, z $\{01\bar{1}1\}$, and r $\{10\bar{1}1\}$-faces.[12] The mixed as-grown $GeO_2-SiO_2$ single-crystal shown on the SEM photograph of Figure 5 is capped with a rhombic pyramidal shape formed of rhombohedron r-faces larger than the z-ones and shows prismatic m-faces forming the long body. This form is very popular among natural quartz crystals but quite an unreported shape for synthetic α-quartz.

For these low-$SiO_2$-substituted $GeO_2$ growth experiments, the rutile-like form was also present when using $K_2O$-$n$$MoO_3$ and $Rb_2O$-$n$$MoO_3$ ($n$ = 2−3) fluxes. Again, the result of the crystal growth experiment using $K_2W_2O_7$ flux was not satisfactory.

From glass solutes with medium- or high-Si-content (close to $Ge_{0.95}Si_{0.05}O_2$ or to $Ge_{0.90}Si_{0.10}O_2$ chemical composition), only the 3 selected potassium molybdate fluxes (see Table 1) were tested.

Selected medium-$SiO_2$-substituted $GeO_2$ single-crystals are presented in the photographs of the Figure 6. Again, colorless, transparent, and well-faceted crystals were obtained in $K_2Mo_3O_{10}$ and $K_2Mo_4O_{13}$ fluxes. The millimeter-sized single-crystals presented a smooth surface roughness and were solvent inclusion-free. Depending on the flux nature, two types of crystals were developed in respect to the shape of their cap. The rhombic pyramidal tops were formed in $K_2Mo_3O_{10}$, Figure 6a whereas in


dx.doi.org/10.1021/ic200661q |*Inorg. Chem.* 2011, 50, 9311–9317

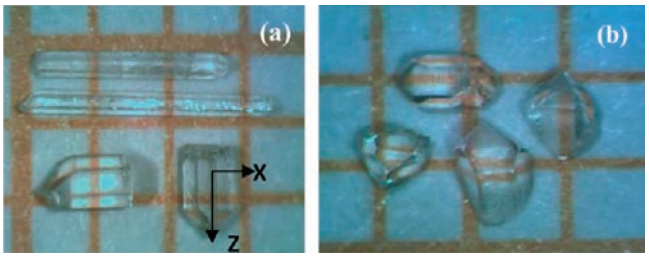


**Figure 6.** Photographs of as-grown medium-$SiO_2$-substituted $GeO_2$ single-crystals in different fluxes; (a) $K_2Mo_3O_{10}$ and (b) $K_2Mo_4O_{13}$, (mm grid).

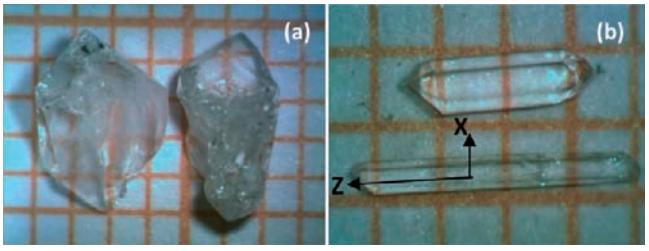


**Figure 7.** Photographs of as-grown high-$SiO_2$-substituted $GeO_2$ crystals grown in (a) $K_2Mo_2O_7$ and (b) $K_2Mo_4O_{13}$, (mm grid).

$K_2Mo_4O_{13}$ the crystals had an ordinary triangular-pyramid cap formed with only r-type faces, Figure 6b.

In $K_2Mo_2O_7$ flux, high-$SiO_2$-substituted $GeO_2$ inclusions-free crystals were obtained with volume as 4.8 × 3.4 × 1.5 $mm^3$ which presented some rough surfaces as shown in Figure 7a. In $K_2Mo_4O_{13}$, transparent hexagonal-prisms were well-formed, Figure 7b, with length as 4.2 mm in the *Z* direction.

In a first approximation, a simple qualitative criterion to approach the crystal quality of these as-grown single-crystals from the experimenter's point of view can be discussed in terms of the level of transparency as determined by a human's eyes. Indeed, single-crystals with a low degree of macroscopic defects due, for example, to chemical impurities, would be characterized by a high-level of "human's eyes" transparency. Any deviation may suggest the presence of higher levels of chemical impurities and structural crystal imperfections as dislocations.

Taking into account this simple experimental criterion, high optical quality $GeO_2$ and $SiO_2$-substituted $GeO_2$ single-crystals with the α-quartz structure were obtained in $MoO_3$-rich fluxes and more particularly with potassium molybdate and rubidium molybdate solvents.

The morphology of $GeO_2$ and its dependence on the growth conditions are of special interest since its piezoelectric properties are directly connected to the crystal slice directions. As shown in Figures 1 and 2, the morphology of pure $GeO_2$ single-crystals is significantly affected when the nature of the flux is changed and the other conditions kept constant. Crystal habit is highly connected to the face growth rate which depends on crystal structure, experimental conditions (temperature, pressure, supersaturation, solvent), and impurities.[18] During layer growth, adsorption on a crystal face of foreign chemical species acting as impurities is susceptible to perturb its atomic arrangement and consequently to modify its reactivity and surface energy and thus to decrease its growth rate. This will induce morphological changes in the grown crystals.

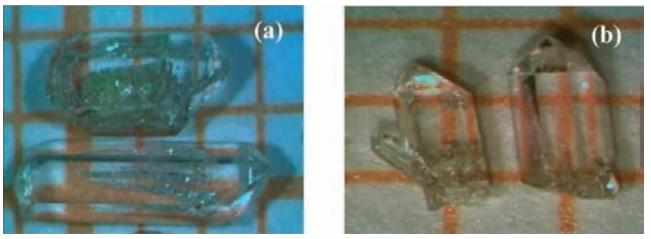


**Figure 8.** Different growth defects encountered in $SiO_2$-substituted $GeO_2$ crystals; (a) flux-inclusion and air bubbles and (b) V-shaped twin, (mm grid).

Furthermore, the substitution of some germanium atoms (ionic radius of $Ge^{4+}$ = 0.53 Å) by silicon atoms (ionic radius of $Si^{4+}$ = 0.41 Å) changes the crystallization process observed for pure $GeO_2$ by leading to the hexagonal-prism-like crystal morphology. Mixed crystals of isomorphous substances usually do not differ very much in habit from the pure components. In hydrothermal conditions, the morphology of spontaneously grown α-$SiO_2$ synthetic crystals in many respects is determined by the experimental conditions. For high supersaturations (temperature difference between zones of dissolution and growth), the quartz crystallizes in a very elongated prism ended by the r faces of the rhombohedron. For very low supersaturations, the effect is less effective, and its habit will be more isometric.[19]

The main macroscopic growth defects encountered among the numerous crystals obtained from each growth experiment were the presence of flux-inclusions, air-bubbles, or V-shaped twin, see photographs in Figure 8.

Most of the trapped gas bubbles in $SiO_2$-substituted $GeO_2$ crystals look like tiny spheres which propagate as a line in the optical direction, see crystal at the bottom of Figure 8a. One explanation of such phenomenon could be that air is introduced when loading the raw materials into the Pt crucible. Because of the absence of forced convection in the melt during the growth experiments, the air moves slowly from the solid−liquid interface to the upper part of the crucible.[20] As a result, a series of gas bubbles are sometimes frozen into the as-grown crystals during the initial stage of growth.

This V-shaped twin crystal, Figure 8b, is considered as a contact twin because of its appearance: two single-crystals seem to be interconnected. The *Z*-growth axis of each individual crystal is close to 35° in this example.

**Characterizations.** The flux-grown crystals of pure $GeO_2$ material and $Ge_{1-x}Si_xO_2$ solid-solution were identified by powder XRD at room-temperature. All reflections in the powder patterns can be indexed on the basis of the trigonal system with a $P3_221$ space group in accordance to the JCPDS card No. 36-1463.[21] No trace of impurity phases was found. See Figure 9 as an illustration which concerns pure $GeO_2$ material.

The lattice parameters given in Table 2 were obtained using the LeBail method with the FullProf computer program for each studied composition.[22,23]

Concerning the pure $GeO_2$ material, the lattice parameters were $a = b$ = 4.98438(3) Å and $c$ = 5.64665(4) Å which are in good agreement with the literature data.[6] As the rate of the Si-substitution increases, both the lattice parameters and the volume decrease as expected.

A chemical analysis of selected $GeO_2-SiO_2$ mixed samples was performed using an EDX microprobe with multipoint sampling to approximate the Si-substitution content and the homogeneity of

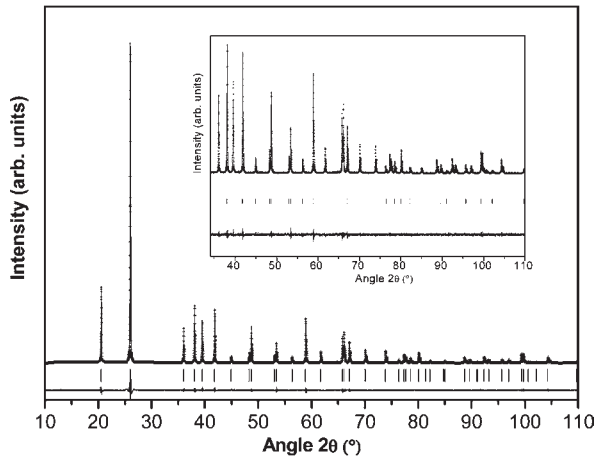


**Figure 9.** Observed (solid line) and calculated (cross) powder XRD pattern of $GeO_2$ material at room temperature. The difference reflection is shown at the bottom. Ticks marks indicate allowed reflection in the $P3_221$ structure.

**Table 2. Lattice Parameters and Cell Volume of Flux-Grown $GeO_2$ and $SiO_2$-Substituted $GeO_2$ Single-Crystals[a]**

| | α-$GeO_2$ | low Si-content | medium Si-content[24] | high Si-content | α-$SiO_2$ |
|---|---|---|---|---|---|
| *a* (Å) | 4.98438(3) | 4.9821(2) | 4.9816(2) | 4.9777(2) | 4.921(1) |
| *c* (Å) | 5.64665(4) | 5.6380(2) | 5.6207(3) | 5.6145(3) | 5.4163(8) |
| *c*/*a* | 1.13287(2) | 1.1317(1) | 1.1280(2) | 1.1279(2) | 1.1007(3) |
| V (Å$^3$) | 121.491(1) | 121.194(8) | 120.80(2) | 120.475(10) | 113.59(4) |

[a] The parameters of hydrothermally-grown α-quartz are also given.[3].

the as-grown crystals, Table 3. EDX spectroscopy is a well-established technique for in situ microanalysis of major and minor elements at concentrations above a few hundred ppm and its accuracy is typically under 1%.

The average Ge and Si contents measured in these controlled $SiO_2$-substituted $GeO_2$ crystals gave the corresponding chemical composition: $Ge_{0.962}Si_{0.038}O_2$ for a low Si-content, $Ge_{0.951}Si_{0.049}O_2$ for a medium Si-content, and $Ge_{0.911}Si_{0.089}O_2$ for a high Si-content.

The silicium distribution at the surface seems to be homogeneous in regard to the accuracy of each measure. Beside the host elements, no other chemical element as those brought by the flux (K, Mo, Cs, Rb, ...) was detected by EDX, see Figure 10 given as an illustration. This could also be due to a too small chemical element content to be detected by this method (below the detection threshold). The presence of foreign elements considered as impurities disturbs the crystallization process and thus induces the formation of structural defects which deteriorate the physical properties of the material.

The collection of the room-temperature infrared data was done on as-grown samples, that is, not polished materials. The 2500−3800 cm$^{-1}$ middle infrared transmission region of pure $GeO_2$ and of selected flux-grown single-crystal with different $SiO_2$ content is shown in Figure 11.

The presence of OH-groups, which decrease the Q-factor of the resonators, was reported in the literature concerning the crystal growth of α-$GeO_2$ by the hydrothermal method.[25] In an infrared spectrum of a $GeO_2$ material containing significant

**Table 3. EDX Microprobe Results in Atomic (%) with Multipoint Sampling on $Ge_{1-x}Si_xO_2$ Mixed Single-Crystals[a]**

| as-grown crystal | Si | Ge |
|---|---|---|
| low Si-content | 1.25 | 31.48 |
| | 1.35 | 31.40 |
| | 1.13 | 31.75 |
| | *1.24(9)* | *31.54(15)* |
| medium Si-content | 1.81 | 36.06 |
| | 1.82 | 35.84 |
| | 1.89 | 35.62 |
| | *1.84(4)* | *35.84(18)* |
| high Si-content | 3.27 | 32.03 |
| | 3.34 | 32.21 |
| | 2.86 | 33.01 |
| | *3.16(21)* | *32.41(43)* |

[a] In italics, the average values with their standard deviation used to determine the Si fraction ($x$) of the $Ge_{1-x}Si_xO_2$ sample.

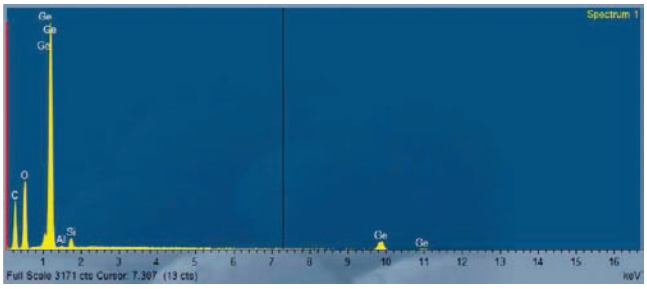


**Figure 10.** EDX spectrum of a crystal grown in the $GeO_2$−$SiO_2$ solid-solution. Detection of Ge (K: 1.188 KeV, L: 9.885 KeV), Si (K: 1.740 KeV), O (K: 0.523 KeV), C from adhesive tape (K: 0.277 KeV) and Al from sample holder (K: 1.486 KeV).

OH-groups, a well-pronounced broad band between 2500 and 3800 cm$^{-1}$ is observed, see Figure 11.

In Figure 11, well-pronounced broad bands characterizing significant OH-groups contamination in the samples are not visible for flux-grown samples. These registered infrared spectra correspond to samples without OH-content. This is an important result for the crystal quality since OH-groups enter the structure network and act as impurities which affect the piezoelectric properties especially at high temperature. Therefore, the flux method is a powerful way to synthesize OH-free $GeO_2$-based materials as already mentioned for flux-grown $GaPO_4$ single-crystals with the α-quartz structure.[26]

In the temperature range from room temperature to 1200 °C, the DSC heating-curves of the $GeO_2$ and $SiO_2$-substituted $GeO_2$ crystals with the α-quartz structure show no other peak than an endothermic feature attributed to the melting of the studied material, Figure 12.

The very interesting result brought to light by this thermal analysis is that these oxide materials do not present a phase transition before melting unlike $SiO_2$ with the well-known α-quartz/$\beta$-quartz transformation close to 573 °C.[27] $GeO_2$ and $SiO_2$-substituted $GeO_2$ crystals with the α-quartz structure are stable from room temperature to at least 1000 °C under inert-atmosphere condition.


dx.doi.org/10.1021/ic200661q |*Inorg. Chem.* 2011, 50, 9311–9317

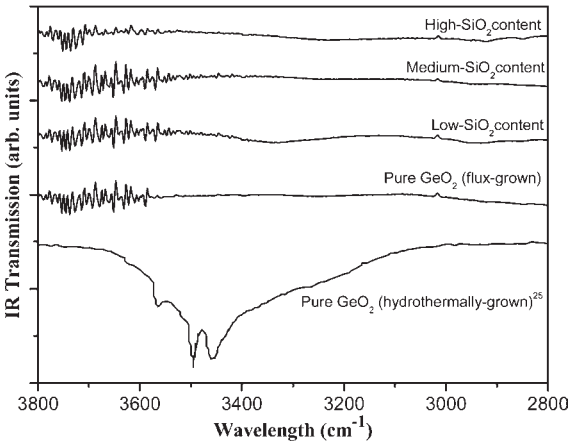


**Figure 11.** Infrared transmission spectra of α-$GeO_2$ (flux- and hydrothermally grown) and mixed $GeO_2$−$SiO_2$ single-crystals.

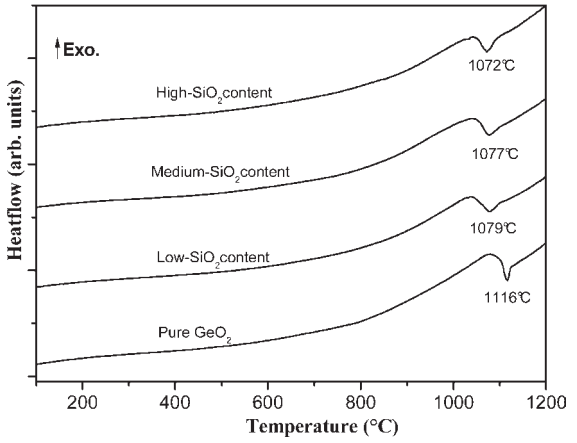


**Figure 12.** DSC heating-curves of flux-grown α-$GeO_2$ and mixed $GeO_2$−$SiO_2$ single-crystals.

It should be noticed that as the Si-substitution increases in the $GeO_2$ crystal structure, the melting temperature decreases as we can see in Figure 12. This is in balance with the solid−liquid transition of the binary $GeO_2$−$SiO_2$ phase diagram.[28]

## CONCLUSION

The important information of the present investigation is that a suitable method and appropriate conditions have been found for the growth of high-quality $GeO_2$-based piezoelectric single-crystals.

Indeed, using the spontaneous nucleation method in selected fluxes, well-faceted, visually colorless, and transparent single-crystals of pure $GeO_2$ and $SiO_2$-substituted $GeO_2$ materials with the α-quartz structure were grown. Flux-grown Si-substituted $GeO_2$ single-crystals present hexagonal-prism morphology with a homogeneous silicon distribution while pure $GeO_2$ is often present with a pseudocubic form. Again, while the number of pure $GeO_2$ crystals obtained after a growth experiment is poor, the substitution of Ge atoms by Si ones increases by a factor of 2 to 3 the crystal's yield of the growth experiment.

Results concerning their thermal behavior and their OH-free content are also very interesting. These flux-grown oxide materials are characterized by an absence of phase transition from room-temperature up to their melting temperature. Neither an α-quartz/β-quartz transition as encountered in $SiO_2$ near 573 °C nor an α-quartz to rutile transformation are present for these $GeO_2$-based materials. This implies that compared to α-$SiO_2$ these germanium oxide materials could be used at more elevated temperature, until 1000 °C. Furthermore, the high temperature growth method used limits the presence of hydroxyl groups in the structure. OH-entities may damage the physical properties of the materials since they act as impurities and decrease the crystalline quality of the single-crystal.

The high crystal quality of these flux-grown $GeO_2$-based single-crystals coupled with their positive thermal behavior show that the flux method is a powerful way to synthesize OH-free materials as already mentioned for isostructural $GaPO_4$ single-crystals.[26]

However, the dimension of the as-grown crystals has to be improved to be able to characterize their piezoelectric and dielectric properties. This could be done using, for example, the Top Seeded Solution Growth (TSSG) technique from seeds.

## AUTHOR INFORMATION

### Corresponding Author

*Phone: (+33) 4 67 14 33 19. Fax: (+33) 4 67 14 42 90. E-mail: pascale.armand@univ-montp2.fr.

## ACKNOWLEDGMENT

We would like to thank Mr. David Maurin (Laboratoire Charles Coulomb, UMII, Montpellier, France) for his help during Infrared measurements, Messrs. Claude Gril and Fréderic Fernandez (Service Commun Microscopie Electronique, UMII, Montpellier, France) for the EDX experiments and Mrs. Dominique Granier (ICGM, UMII, Montpellier, France) for her assistance during powder X-ray pattern recording.

## REFERENCES

(1) Grimm, H.; Dorner, B. *J. Phys. Chem. Solids* **1975**, *36*, 407.
(2) Philippot, E.; Goiffon, A.; Ibanez, A.; Pintard, M. *J. Solid State Chem.* **1994**, *110*, 356.
(3) Glinnemann, J.; King, H. E., Jr.; Schulz, H.; Hahn, Th.; La Placa, S. J.; Dacol, F. *Z. Kristallogr.* **1992**, *198*, 177.
(4) Laubengayer, A. W.; Morton, D. S. *J. Am. Chem. Soc.* **1932**, *54*, 2303.
(5) Kotera, Y.; Yonemura, M. *Trans. Faraday Soc.* **1963**, *59*, 147.
(6) Haines, J.; Cambon, O.; Philippot, E.; Chapon, L.; Hull, S. *J. Solid State Chem.* **2002**, *166*, 434.
(7) Demianets, L. N. *Prog. Cryst. Growth Charact. Mater.* **1990**, *21*, 299.
(8) Glushkova, T. M.; Kiselev, D. F.; Makhina, I. B.; Firsova, M. M.; P.Shtyrkova, A. *Moscow Univ. Phys. Bull.* **1992**, *17*, 55.
(9) Balitsky, D. V.; Balitsky, V. S.; Pushcharovsky, D. Y.; Bondarenko, G. V.; Kosenko, A. V. *J. Cryst. Growth* **1997**, *180*, 212.
(10) Finch, C. B.; Clark, G. W. *Am. Mineral.* **1968**, *53*, 1394.
(11) Tarr, W. A.; Lonsdale, J. T. *Am. Mineral.* **1929**, *14*, 50.
(12) Dowty, E. *Am. Mineral.* **1976**, *61*, 448.
(13) Hartman, P.; Perdok, W. G. *Acta Crystallogr.* **1955**, *8*, 49.
(14) Hemmerling, J.; Hergt, R. *Kristall Tech.* **1980**, *15*, 795.
(15) Elwell, D.; Scheel, H. J. *Crystal Growth from High Temperature Solutions*; Academic Press: New York, 1975; pp 261−264.
(16) Swets, D. E. *J. Cryst. Growth* **1971**, *8*, 311.
(17) Frondel, C. The System of Mineralogy (DANA). In *Silica Minerals*; J. Wiley: New York, 1962; Vol. III.
(18) Philippot, E.; Goiffon, A.; Ibanez, A. *J. Cryst. Growth* **1996**, *160*, 268.

(19) Hartman, P. *B. Minéral.* **1978**, *101*, 195.
(20) Xianjun, Wu; Jiayue, Xu; Weiqing, J. *Mater. Charact.* **2005**, *55*, 143.
(21) The Joint Committee on Powder Diffraction Standards Card No. 36-1463.
(22) Rodriguez-Carvajal, J. *Phys. B* **1993**, *192*, 55.
(23) Roisnel, T.; Rodriguez-Carvajal, J. *Mater. Sci. Forum* **2001**, *378*, 118.
(24) Armand, P.; Clément, S.; Balitsky, D.; Lignie, A.; Papet, P. *J. Cryst. Growth* **2011**, *316*, 153.
(25) Pey, F. Ph.D. Thesis, Université Montpellier II, Montpellier, France, 2004.
(26) Beaurain, M.; Armand, P.; Papet, P. *J. Cryst. Growth* **2006**, *294*, 396.
(27) Dolino, G. *Phase Transitions.* **1990**, *21*, 59.
(28) Miller, W. S.; Roy, R.; Shafer, E. C.; Dachille, F. *Am. Mineral.* **1963**, *48*, 1024.